Coordination Modulation Method to Prepare New MOF-based CO-Releasing Materials

Francisco J. Carmona,[†] Carmen R. Maldonado,[†] Shuya Ikemura,[⊥,#] Carlos C. Romão,[‡,§] Zhehao Huang,[∥] Hongyi Xu,[∥] Xiaodong Zou,[,∥] Susumu Kitagawa,[⊥] Shuhei Furukawa,[*,⊥,#] and Elisa Barea[*,†]*

[†] Department of Inorganic Chemistry, University of Granada, Av. Fuentenueva S/N, 18071 Granada, Spain.

[‡] Instituto de Tecnologia Química e Biológica, Universidade Nova de Lisboa, Av. da República, EAN, 2780-157 Oeiras, Portugal.

[§] Proterris (Portugal), Instituto de Biologia Experimental e Tecnológica, Av. da República, EAN, 2780-157 Oeiras, Portugal.

[∥] Department of Materials and Environmental Chemistry, Stockholm University, Berzelii Centre EXSELENT on Porous Materials, and Inorganic and Structural Chemistry, SE-106 91 Stockholm, Sweden.

[⊥]Institute for Integrated Cell-Material Sciences (WPI-iCEMs), Kyoto University, Yoshida, Sakyo-ku, Kyoto 606-8501, Japan.

[#] Department of Synthetic Chemistry and Biological Chemistry, Graduate School of Engineering, Katsura, Nishikyo-ku 615-8510, Japan.

KEYWORDS. Carbon monoxide, Metal organic framework, Solid-state materials, Guest inclusion, Continuous rotation electron diffraction.

ABSTRACT. Aluminium-based metal-organic frameworks, $[Al(OH)(SDC)]_n$, (H_2SDC: 4,4'-stilbenedicarboxylic acid) also known to be CYCU-3 were prepared by means of the coordination modulation method to produce materials with different crystal size and morphology. In particular, we screened several reagent concentrations (20-60 mM) and modulator/ligand ratios (0-50), leading to twenty CYCU x_y materials (x: reagent concentration, y = modulator/ligand ratio) with different particle size and morphology. Noteworthy, the use of high modulator/ligand ratio gives rise to a new phase of CYCU-3 (CYCU-3' x_50 series) which was structurally analyzed. Afterwards, and in order to test the potential of these materials as CO-prodrug carriers, we selected three of them to adsorb the photo- and bioactive CO-releasing molecule (CORM) ALF794 $[Mo(CNCMe_2CO_2H)_3(CO)_3]$ ($CNCMe_2CO_2H$ = 2-isocyano-2-methyl propionic acid): *i)* CYCU-3 20_0, particles in the nanometric range; *ii)* CYCU-3 50_5, bar-type particles with heterogeneous size and *iii)* CYCU-3' 50_50, a new phase analogous to pristine CYCU-3. The corresponding hybrid materials were fully characterized revealing that CYCU-3 20_0 with the smallest particle size was not stable under the drug-loading conditions. Regarding the other two materials, similar ALF794 loadings were found (0.20 and 0.19 CORM/MOF molar ratios for ALF794@CYCU-3 50_5 and ALF794@CYCU-3' 50_50, respectively). In addition, these hybrid systems behave as CO-releasing materials (CORMAs), retaining the photoactive properties of pristine CORM in both phosphate saline solution and solid state. Finally, metal leaching studies in solution confirmed that ALF794@CYCU-3' 50_50 shows a good retention capacity towards the potentially toxic molybdenum fragments (75 % of retention after 72 hours) which is the lowest value reported for a MOF-based CORMA to date.

INTRODUCTION

Since pioneering work of Nobel laureates Furchogtt, Ignarro and Murad concerning nitric oxide (NO) as an important biosignaling molecule in the cardiovascular system,[1,2] significant attention has been paid on the physiological and potential therapeutic role of other endogenously produced small gas molecules, such as carbon monoxide (CO)[3] and hydrogen sulphide (H_2S).[4] Among these gases, CO exhibits lower reactivity than NO or H_2S acting only as a ligand for metalloproteins. This different behaviour plays an advantage in biomedical applications as CO is most likely to reach the cellular target intact.[5,6] In this context, carbon monoxide has already shown anti-hypertensive, anti-inflammatory and cell-protective effects, demonstrating its potential as a therapeutic tool if supplied exogenously in low concentrations.[3,7] The easiest administration route for this gas molecule into the body is the inhalation of CO/air mixtures. Indeed, several clinical trials have been completed or are currently in progress in order to evaluate the safety and efficacy of inhaled CO against several diseases.[8,9] However, this delivery strategy lacks specificity as CO distribution is determined by fixed partition coefficients between the different body fluids and tissues. In addition, the higher affinity of CO to haemoglobin compared to oxygen, as well as its poor solubility in water, means that high doses of inhaled CO are required to obtain a beneficial effect with the concomitant associated safety risk.[10]

In order to overcome these drawbacks, Motterlini *et al.* introduced the concept of CO-releasing molecules (CORMs) and demonstrated, for the first time, the feasibility of using metal carbonyls to release CO inducing beneficial vascular effects.[11] Since then, several CO pro-drugs have been designed from readily available and highly tailorable metal and ligand precursors in order to control the number of CO molecules released and/or the triggering mechanism of CO-delivery (e.g. light, physiological changes, enzyme activation).[12] Unfortunately, despite the high versatile

chemistry of these pro-drugs, most of them have low solubility and/or stability in physiological media, fast CO release and undesirable toxic effects associated to their decarbonylation products, which prevent their clinical development.[13]

One smart approach to overcome the above mentioned weaknesses is the combination of existing CO-releasing molecules with biocompatible solids, resulting in CO-releasing materials (CORMAs).[14–23] Such hybrid systems are expected to maintain the triggering properties of the pristine CORM, improve its chemical stability in the physiological medium and retain the potentially toxic co-ligand fragments. Besides, for biomedical applications, apart from toxicity issues, particle size and morphology of the carrier should be taken into account not only to assess the appropriate administration route (e.g. intravenous via requires particle diameter less than 200 nm[24] while bigger particles, even in the micrometric range, may be used for oral administration or topical applications) but also to exert a certain control on cargo, drug delivery process and chemical stability of the resulting hybrid material.[25]

In this context, metal-organic frameworks (MOFs) have recently gained especial importance as promising CO carriers. However, to the best of our knowledge, only four CORMAs based on MOFs have been published to date. The first CO-delivery system using a MOF as a platform was prepared by Metzler-Nolte et al.[26] In this case, carbon monoxide was reversibly captured on the unsaturated coordination sites of MIL-88B-Fe derivatives to be delivered later by simple degradation of the matrixes. Afterwards, some of us, Maldonado, Barea *et al.*, prepared a photoactive CORM@MOF system by a cation exchange methodology on the biocompatible bioMOF-1.[27] However, the scarce stability of the resulting hybrid material in buffered solution led to the complete leaching of the CORM in a short timeframe. More recently, Furukawa *et al.* have designed a covalently attached CORM@MOF system by embedding a photoactive

manganese complex into a robust Zr(IV)-MOF. In this case, CO delivery was monitored in the solid state.[28] Finally, Barea, Maldonado *et al.* reported for the first time the one-pot synthesis of a new CORM@MOF system by incorporating the CORM $[Mo(CNCMe_2CO_2H)_3(CO)_3]$ (ALF794)[29] into the textural mesopores of the hierarchical structure of $[Zn_2(dhtp)]$ (dhtp = 2,5-dihydroxyterephtalate) (h-ZnCPO). In this case, the hybrid system behaves as a photoactive CORMA retaining most of the potentially toxic decarbonylation fragments.[30] These examples showed that porous frameworks with exceptional high surface to volume ratio allow i) elevated CO payloads, ii) trapping of the decarbonylation products generated after activation, and iii) tuning of CO-delivery kinetics. Additionally, both particle size and morphology of MOFs can be controlled through different synthetic methodologies (e.g. mechanochemistry, ultrasound-assisted synthesis, microemulsion synthesis).[31,32] Among them, conventional solvothermal synthesis assisted by the coordination modulation method (CMM), is a relatively simple and versatile strategy based on the use of capping reagents to modulate the crystal growth process.[25] In this regard, particularly interesting is the above mentioned pioneering work of Furukawa *et al.*, which focused on the influence of particle size over the CO releasing properties of the CORMA $MnBr(bpydc)(CO)_3$@UiO-67 (bpydc = 5,5'-dicarboxylate-2,2'-bipyridine).[28]

Taking into account this background, in this work, we show the feasibility to control particle size and morphology in $[Al(OH)(SDC)]_n$ (H_2SDC: 4,4'-stilbenedicarboxylic acid) (CYCU-3)[33] by means of CMM. With this aim, we screened different reagent concentrations and modulator/ligand ratios. As a result, CYCU-3 materials with different particle features were isolated including a new crystalline phase (CYCU-3' 50_50), for which a structural model based on a defective and more dense structure than pristine CYCU-3 was proposed. Then, taking into account that CYCU-3 is composed by low toxic Al(III) ions and its structure is based on one-

dimensional mesopores (~ 3 nm) that are able to host bulky molecules, we decided to use it as a platform to obtain new CO-releasing materials. Thus, the non-toxic air-stable CORM ALF794 ($Mo(CNCMe_2CO_2H)_3(CO)_3$), which has demonstrated efficacy in an animal model of acute liver failure,[29] and can also be activated by light, was selected as a model drug to be loaded in three CYCU-3 materials. The influence of structure, crystal size and morphology over the resulting CO-releasing properties, including payload, CO-delivery and matrix stability were also evaluated (Scheme 1).

Scheme 1. Incorporation of the model CO-prodrug ALF794 inside CYCU-3 porous matrix and CO release upon photoactivation.

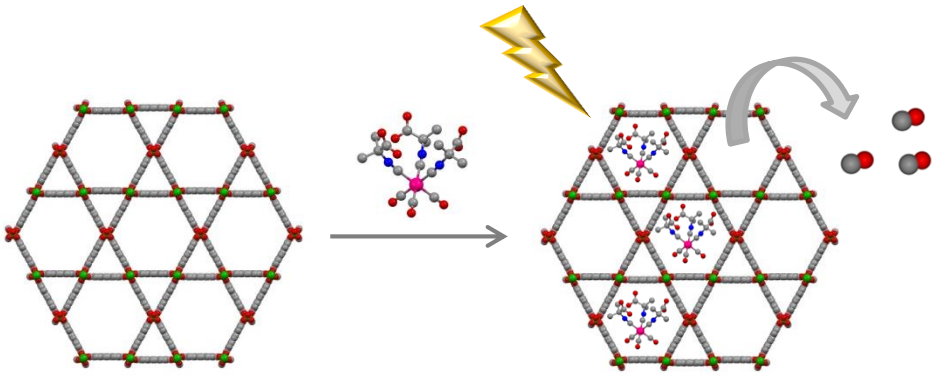

EXPERIMENTAL SECTION

All chemicals were commercially available and used without further purification. The CORM ALF794 [$Mo(CO)_3(CNCMe_2CO_2H)_3$] ($CNCMe_2CO_2H$ = tris(2-isocyano-2-methyl propionic acid) was provided by Proterris (Portugal) Lda.

Synthesis of CYCU-3 materials $[Al(OH)(SDC)]_n$ (H_2SDC: 4,4'-stilbenedicarboxylic acid). Several screenings were carried out in order to evaluate the influence of the synthetic conditions,

namely reagents concentration and modulator/ligand ratio, over the particle properties in CYCU-3. In a typical reaction, an equimolar mixture of $Al(NO_3)_3 \cdot 9H_2O$ and H_2SDC (with concentrations varying from 20, 30, 40, 50 and 60 mM) in 750 μL of *N*,*N*-dimethylformamide (DMF) was mixed with the modulator (acetic acid to ligand ratio used: 0-1, 5-1, 20-1 and 50-1) and placed in a 1 mL teflon lined reactor. The slurry was heated at 190 ºC for 72 hours, and cooled down to room temperature during 6 hours. The resulting white solid was washed with DMF (3 x 1 mL), collected by centrifugation (10 min /3500 rpm) and dried at 90 ºC under vacuum. As a result, twenty new materials were isolated (namely, CYCU-3 x_y, x: reagent concentration (mM), y: modulator/ligand ratio) and characterized by X-ray powder diffraction and Scanning Electron Microscopy. From this preliminary screening, three of these materials (CYCU-3 20_0, CYCU-3 50_5 and CYCU-3' 50_50) were selected and scaled-up in order to study their potential properties as CORMAs (see discussion section).

Scale-up synthesis of CYCU-3 20_0. A suspension of 75 mg (0.2 mmol) of $Al(NO_3)_3 \cdot 9H_2O$ and 53.6 mg (0.2 mmol) of H_2SDC in 10 mL of DMF was transferred to a 23 mL teflon lined reactor. The slurry was heated at 190 ºC for 72 hours and cooled down to room temperature in 6 hours. The white solid was washed with DMF (3 x 10 mL), collected by centrifugation (10 min/3500 rpm) and dried at room temperature. The as-synthetized material was further washed in order to remove the potential unreacted ligand, which could be trapped inside the cavities. Thus, the corresponding solid was suspended in DMF (5 mg per mL), heated in a microwave-assisted reactor (50 ºC, 15 minutes) and collected by centrifugation (10 min/3500 rpm). This process was done in triplicate. Anal. Calc. for CYCU-3 20_0 $[Al(OH)(C_{16}O_4H_{10})](H_2O)_{1.1}(C_3H_7NO)_{0.1}$: N, 0.42; C, 58.03; H, 4.15. Found: N, 0.39; C, 60.11; H, 4.24. Residue (Al_2O_3) (calc./exp.): 16.13/15.88%.

Scale-up synthesis of CYCU-3 50_5. The material CYCU-3 50_5 was prepared and isolated following the same procedure than for CYCU-3 20_0. In this case, a suspension of 187.6 mg (0.5 mmol) of $Al(NO_3)_3 \cdot 9H_2O$ and 134.1 mg (0.5 mmol) of H_2SDC in 9.86 mL of DMF was mixed with 0.14 mL (2.5 mmol) of acetic acid. Anal. calc. for CYCU-3 50_5 $[Al(OH)(C_{16}O_4H_{10})_{0.75}(CH_3COO)_{0.5}](H_2O)_{1.5}(C_3H_7NO)_{0.18}$: N, 0.80; C, 51.89; H, 4.59. Found: N, 0.77; C, 51.31; H, 4.35. Residue (Al_2O_3) (calc./exp.): 16.27/18.22%.

Scale-up synthesis of CYCU-3' 50_50. The material CYCU-3' 50_50 was prepared and isolated following the same procedure than for CYCU-3 20_0. In this case, a suspension of 187.6 mg (0.5 mmol) of $Al(NO_3)_3 \cdot 9H_2O$ and 134.1 mg (0.5 mmol) of H_2SDC in 8.6 mL of DMF was mixed with 1.4 mL (25 mmol) of acetic acid. Anal. calc. for CYCU-3' 50_50 $[Al(OH)(C_{16}O_4H_{10})_{0.55}(CH_3COO)_{0.9}](C_3H_7NO)_{0.04}$: N, 0.23; C, 52.23; H, 3.88. Found: N, 0.29; C, 52.73; H, 3.58. Residue (Al_2O_3) (calc./exp.): 20.68/22.10%.

Evacuation/Activation of CYCU-3 and CYCU-3' materials. Prior to CORM loading, the selected CYCU-3 and CYCU-3' matrices were outgassed (150 ºC, 10^{-4} bar) for 24 hours. Under these conditions, the complete removal of solvent guest molecules was achieved and empty pores ready for drug adsorption were obtained.

Loading of ALF794 into CYCU-3 matrices. The loading of the CORM inside the pores of the selected CYCU-3 matrices, namely CYCU-3 20_0, CYCU-3 50_5 and CYCU-3' 50_50, was carried out by solid-liquid impregnation at room temperature. In a typical procedure, 10 mL of a methanol solution of ALF794 (100 mg, 0.19 mmol) was added to a suspension of previously activated CYCU-3 matrix (100 mg in 10 mL of MeOH). The mixture was stirred until complete evaporation of the solvent (*ca*. 10 hours). Then, the solid was washed with methanol (3 x 10

mL), collected by centrifugation (3500 rpm/10 min) and dried at room temperature. Following the same procedure, additional experiments in absence of ALF794 (100 mg of CYCU-3 matrix in 20 mL of MeOH) were also performed in order to evaluate the stability of the three selected matrices during the impregnation process. All manipulations were carried out in darkness to avoid the undesirable photoactivation of the CORM.

XR fluorescence of ALF794@CYCU-3 20_0. Mo/Al molar ratio=0.14. Residue (exp.) 19.34%.

XR fluorescence of ALF794@CYCU-3 50_5. Mo/Al molar ratio=0.20. Residue [$(Al_2O_3)_{0.5}$ $(MoO_2)_{0.20}$] (calc./exp.): 18.87/20.40%.

XR fluorescence of ALF794@CYCU-3' 50_50 Mo/Al molar ratio= 0.19. Residue [$(Al_2O_3)_{0.5}(MoO_2)_{0.19}$] (calc./exp.): 19.85/18.79 %.

CO detection in the solid-state. A suspension in pentane of the sample was repeatedly spin-coated on a glass substrate. The weight of the sample was accurately determined using a precision scale (typical weights 0.9-1.1 mg). The sample was placed in a custom-made chamber with a glass window on the top and irradiated with a 300 W xenon lamp (Asahi Spectra Max-303 equipped with a 235-385 nm ultraviolet module and x 1.0 collimator lens). The light intensity was 50 $mWcm^{-2}$. The released CO gas from CORMA was carried to the CO detector (HALO 3 TM trace gas analyser from Tiger Optics) by N_2 flow (500 ml min^{-1} flow rate).

Leaching studies of ALF794@CYCU-3 50_5 and ALF794@CYCU-3' 50_50 in PBS under visible light. In order to evaluate the ability of the hybrid materials to retain the metal fragments inside the pores, suspensions of ALF794@CYCU-3 50_5 (24 mg L^{-1}) and ALF794@CYCU-3' 50_50 (15 mg L^{-1}) in 10 mM PBS (Phosphate Buffered Saline) were prepared. Samples were

incubated at 37 °C under visible light for 6, 24 and 72 hours (using a fluorescent lamp, luminous flux: 600 lm; color temperature: 4000 K, distance between lamp and cuvette: 5 cm). At each time, the supernatant was collected by centrifugation (3500 rpm / 10 min) and filtered off (nylon filter membrane, 0.2 μm). The concentration of Mo was quantified by ICP-OES.

Structural characterization of CYCU-3' 50_50 by Continuous Rotation Electron Diffraction (CRED). In order to analyse nature of the isolated CYCU-3' x_50 materials, we carried out a structural study of CYCU-3' 50_50 by Continuous Rotation Electron Diffraction (CRED). With this aim, the sample was dispersed in acetone and a droplet of the suspension was transferred onto a carbon-coated copper grid. Three-dimensional (3D) CRED data of CYCU-3' 50_50 was collected at 200 kV on a JEOL JEM2100 TEM using the Timepix pixel detector QTPX-262k (512 x 512 pixels, pixel size 55 μm, Amsterdam Sci. Ins.). A single-tilt tomography sample holder was used for the data collection, which could tilt from -70° to +70°. The electron beam was fully spread and covered the whole phosphorus screen. The aperture used for CRED data collection was about 1.0 μm in diameter. Electron diffraction (ED) data where acquired in a selected area using continuous electron diffraction mode. The speed of goniometer tilt was 0.074°/s, and the exposure time was 50 ms per frame. 924 ED frames were collected within 1 minute, covering a tilt range from 50.6° to -16.4°. The 3D reciprocal lattice of CYCU-3' 50_50 was reconstructed from the ED frames using the RED – data pro-cessing software package.

Other equipment. XRPD data were collected on a Bruker D2-PHASE diffractometer (2θ) using CuKα radiation (λ = 1.5418 Å) and LYNXEYE detector (University of Granada), or in a SmartLab Rigaku diffractometer using CuKα radiation (λ = 1.5418 Å) (WPI-iCEMs, Kyoto University). Thermogravimetric analysis were performed using a Mettler Toledo TGA/DSC STAR system under oxygen flow (20 mL min^{-1}) running from RT to 900 ºC with a heating rate

of 20 °C min^{-1} (CIC, University of Granada). N_2 adsorption isotherms were measured at 77 K on a Micromeritics Tristar 3000 volumetric instrument. Prior to isotherm acquisition, the matrices were activated and outgassed (150 ºC, 10^{-4} bar) for 24 hours (University of Granada). Infrared spectra were collected in a Fourier transform infrared spectrophotometer (FT-IR) Bruker Tensor 27, using KBr as dispersing agent (University of Granada). Elemental (C, H, N, S) analyses were obtained in a Flash EA1112 CHNS-O (Centre of Scientific Instrumentation, University of Jaén). The molar ratio between Al and Mo was determined via X-ray fluorescence (XRF) spectrometry in a Rigaku NEX CG equipped with a palladium tube as the source of radiation. XRF measurements were performed onto powder samples. Inductively Coupled Plasma Optic Emission Spectrometry analysis (ICP-OES) was carried out in an OPTIMA 7300 DV (SCAI, University of Málaga). Continuous rotation electron diffraction data of CYCU-3' 50_50 was collected at 200 kV on a JEOL JEM2100 Transmission Electron microscope (TEM) using a Timepix pixel detector QTPX-262k (Stockholm University). TEM images and Energy Dispersive X-ray (EDX) elemental mapping were performed using a HAADF FEI TITAN G2 microscope, with a FEI system to carry out chemical analysis (CIC, University of Granada) while SEM images were recorded using a JEOL-JSM-7001F microscope (WPI-iCEMs, Kyoto University). In both cases, samples were prepared by dispersing a small amount of the material (3 mg) in absolute ethanol (1 mL) followed by sonication for 10 min and deposition on a copper grid (TEM) or on a piece of glass (SEM). In the latter case, the sample was coated with Osmium before acquisition.

RESULTS AND DISCUSSION

Control on size and morphology of $[Al(OH)(SDC)]_n$ (CYCU-3) particles

We selected the porous metal-organic network $[Al(OH)(SDC)]_n$ (H_2SDC: 4,4'-stilbenedicarboxylic acid) (CYCU-3) in order to modulate the size and morphology of its particles by using the coordination modulation method (CMM).[25] The use of this strategy allows the preparation of materials with different particle features, which may have influence on the final properties of the prepared CO-releasing materials (e.g. drug cargo, stability and CO-delivery properties). Regarding the CYCU-3, it was firstly synthesized by Lin *et al.*,[33] and its structure is based on Al(III) ions bound to dicarboxylate organic spacers SDC and hydroxide anions acting as bridges, leading to the Kagomé topologies. As a result, two types of cavities are formed, namely, hexagonal mesopores (~ 3 nm) and triangular micropores (~ 1.4 nm). Thus, both size and spatial distribution of CYCU-3 mesopores, leading to one-dimensional channels along the *c* axis, will favour the incorporation and diffusion of bulky guest molecules, making this MOF a suitable vehicle for the loading and release of CO-releasing molecules. Regarding toxicity issues, it is well known the low toxicity of aluminium ions (Oral LD_{50} for Al(III) in rats: 286 mg Kg^{-1}; daily Al(III) requirement in humans: 7.2 mg per day)[34] while, to the best of our knowledge, no biological investigations related to CYCU-3 or 4,4'-stilbenedicarboxylic acid have been reported to date. However, a recent study by Fairen-Jimenez *et al.* pointed forward to certain *in vitro* cytotoxicity of a Zr(IV) MOF containing 4,4'-stilbenedicarboxylate ligands.[35] Noteworthy, in order to prepare CYCU-3 materials, the CMM was selected as the synthetic strategy mainly for two reasons: *i)* firstly, the moderate to harsh reaction conditions (solvothermal synthesis at 190 °C) needed for the preparation of CYCU-3 prevent the use of other synthetic routes, such as mechanochemical or ultrasonic assisted methods; and *ii)* secondly,

the structure of this MOF exhibits two different metal-ligand interaction modes (Al-OH, Al-SDC), allowing an anisotropic modulation during the crystallization process. In this sense, acetic acid was selected as modulator because it is miscible with *N*,*N*-dimethylformamide, the solvent used in the preparation of CYCU-3, and can compete with the carboxylic organic spacer H_2SDC to coordinate to Al(III) metal ions.

Once the synthetic methodology was selected, we decided to study the influence that reagent concentration and modulator/ligand ratio have on both size and morphology of the resulting CYCU-3 materials (Scheme 2).

Scheme 2. Preparation of different CYCU-3 materials using the coordination modulation method.

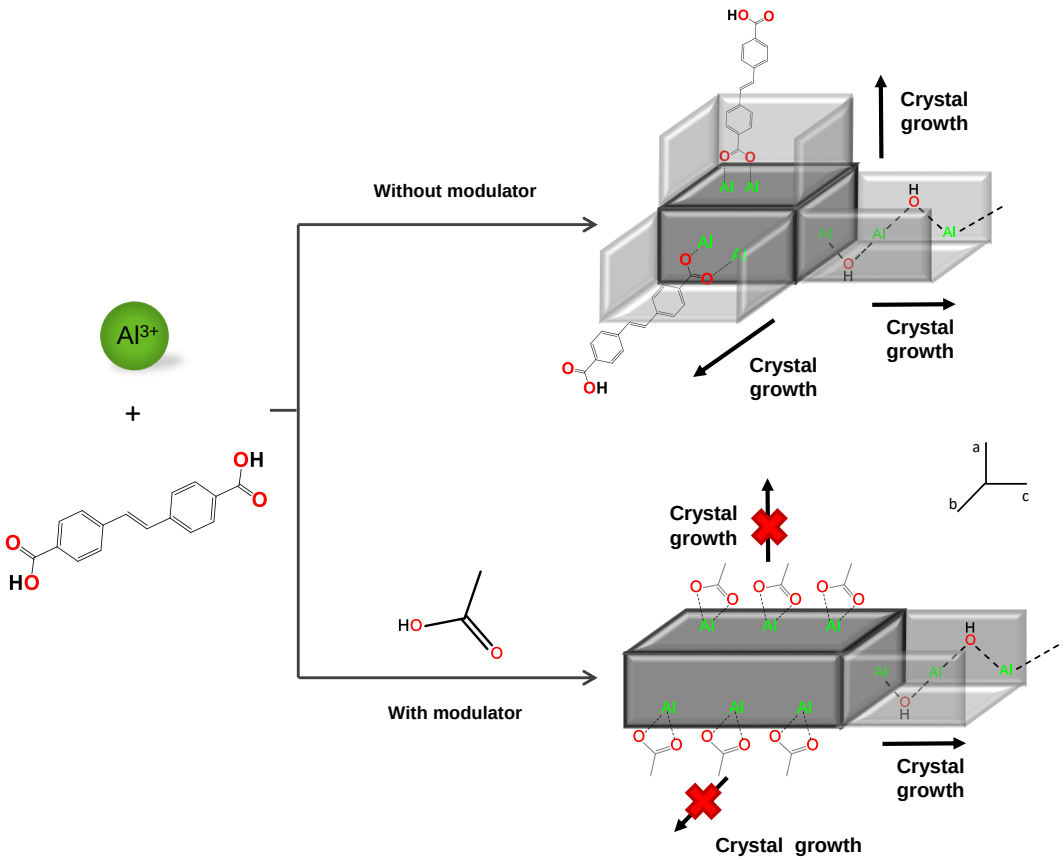

Influence of reagents concentration

In the absence of modulator, different equimolar amounts (20, 30, 40, 50 and 60 mM) of aluminium(III) nitrate and 4,4'-stilbenedicarboxylic acid were reacted in *N*,*N*-dimethylformamide (DMF) by heating the mixtures up to 190 °C for 3 days. In all cases, a white precipitate was obtained, which was thoroughly washed with DMF and allowed to dry at 90 °C under vacuum (see Experimental Section). As a result, five samples were successfully isolated, namely, CYCU-3 20_0, CYCU-3 30_0, CYCU-3 40_0, CYCU-3 50_0 and CYCU-3 60_0 (CYCU-3 x_y, x: reagent concentration (mM), y: modulator/ligand ratio). The crystallinity of the above mentioned materials was analyzed by powder X-ray diffraction (PXRD) measurements. As it is shown in Figure 1, when the most diluted concentration of reagents was used (20 mM) a poorly crystalline material (CYCU-3 20_0) was obtained. In contrast, more crystalline solids were recovered when using higher reagent concentrations (30-60 mM).

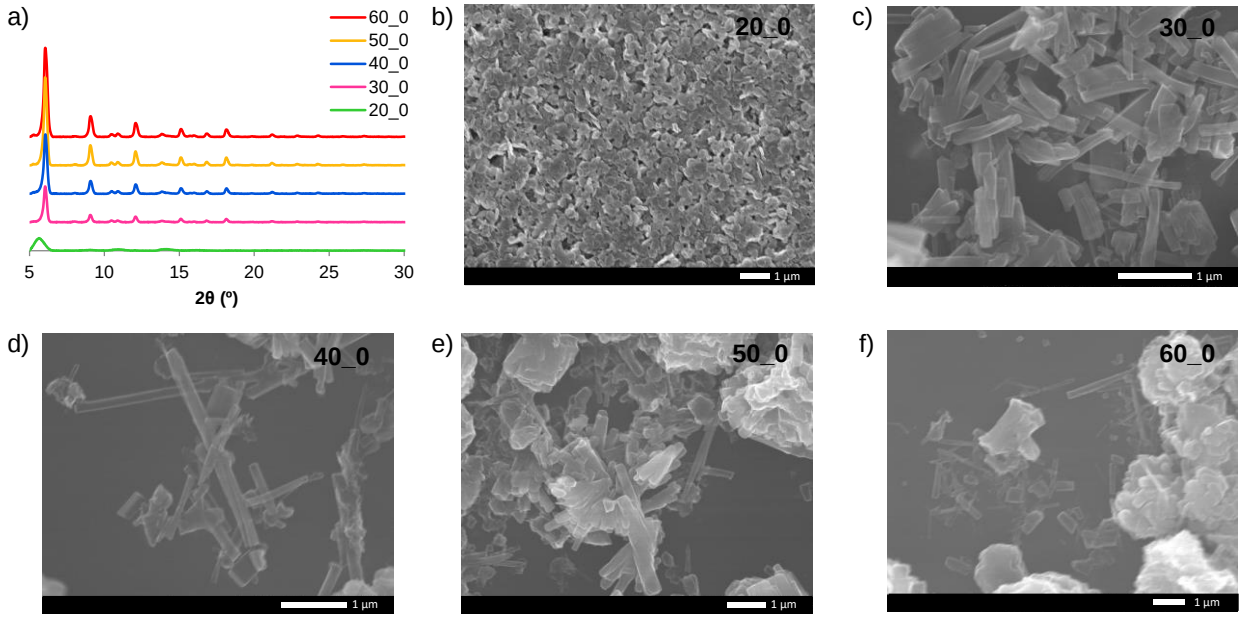

Figure 1. a) X-ray powder diffractograms and b-f) SEM images of CYCU-3 materials prepared in absence of modulator (CYCU-3 x_y, x: reagent concentration (mM), y: modulator/ligand ratio).

Both particle size and morphology of these five materials were examined by Field Emission Scanning Electron Microscopy (FESEM). FESEM images showed that CYCU-3 20_0 is composed by particles in the nanometric range (<100 nm), with pseudo-spherical morphology. Indeed, these particle features are in agreement with the PXRD pattern of this system that showed wide and low intense reflections characteristic of nanometric materials. Besides, the rest of solids comprised mainly particles with bar-like morphology in the micrometric range. It should be noted that when higher concentrations of the reactants are used, more heterogeneous materials including agglomerates are obtained.

Influence of modulator concentration

After analyzing the influence of reagents concentration, different acetic acid/ligand molar ratios (y = 5, 20 and 50) were tested maintaining the previously selected reagent concentrations (20, 30, 40, 50, 60 mM). Thus, other fifteen new CYCU-3 materials were obtained and characterized. On one hand, PXRD studies revealed that increasing amounts of modulator do not improve the crystallinity of the resulting CYCU-3 20_y materials (Figure S1). On the other hand, crystallinity of the rest of isolated solids highly depends on the modulator ratio, showing a similar trend for the tested reagent concentrations (30, 40, 50 and 60 mM). In fact, no changes in the PXRD patterns, in comparison to pristine CYCU-3 published by Lin *et al.* (CYCU-3 40_5),[33] were observed when 5 or 20 acetic acid/ligand molar ratios were used. However, the use of acetic acid with 50 times greater concentration than that of the ligand, always yielded materials with low

crystallinity (CYCU-3' 30_50, CYCU-3' 40_50, CYCU-3' 50_50 and CYCU-3' 60_50) (Figure 2). In addition, the above mentioned systems showed a slight displacement of the most intense reflection to lower angle (from $2\theta = 6.02°$ to 5.62°), which might be indicative of the formation of a new phase (see discussion below). Furthermore, FESEM images confirmed that when the modulator ratio is increased, longer needles are obtained in all cases (Figure S2). This fact can be explained taking into account the structure of CYCU-3, where Al(III) ions are connected through OH bridges giving rise to 1D chains extended along the *c* axis. Additionally, these secondary building units are linked through the SDC linkers, leading to the formation of monodimensional channel structures with hexagonal and triangle shapes. Thus, the addition of modulator has no influence on the Al-OH interactions and, therefore, does not limit crystal growth along the *c*-axis. Nevertheless, acetic acid molecules can compete with organic spacers to coordinate to Al(III) ions, modifying the coordination equilibrium and, consequently, increasing the length/width ratio of the resulting particles. Indeed, this hypothesis is confirmed by the presence of a small amount of acetate, mainly distributed along the surface of the particles, in the corresponding elemental analysis of CYCU-3 50_5 and CYCU-3' 50_50 materials.

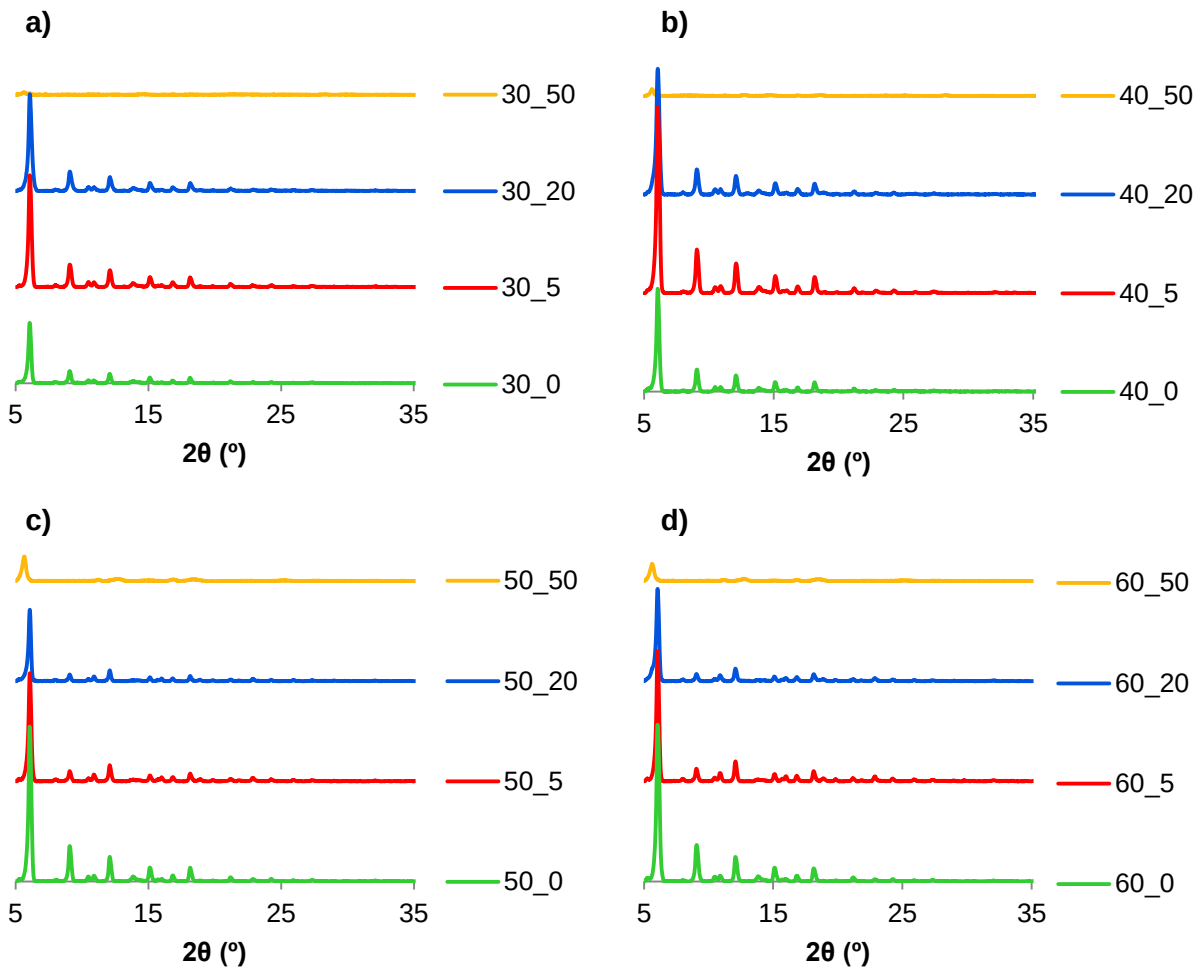

Figure 2. X-ray powder diffractograms of CYCU-3 materials prepared using different reagent concentrations (x= 30 (a), 40 (b), 50 (c) and 60 mM (d)) and increasing acetic acid/ligand ratios (y= 0, 5, 20 and 50).

Structural studies of the new phase CYCU-3'

As mentioned before, and in order to further clarify the nature of the isolated CYCU-3' x_50 materials, we modelled CYCU-3' 50_50 structure by continuous rotation electron diffraction (*c*RED). For this purpose, images of the CYCU-3' 50_50 material were obtained by transmission electron microscopy (TEM) and the electron diffraction data of a selected area (ED) were

recorded. The crystals have long ribbon-like morphology (Figure S3), as previously observed in the corresponding SEM images (Figure S2). The 3D reciprocal lattice of CYCU-3' 50_50 was reconstructed from the ED frames (Figure S4) and used for the determination of the unit cell parameters (a = 16.35 Å, b = 62.15 Å, c = 6.73 Å, α = 89.7°, β = 94.5°, and γ = 88.1°). These values showed some differences, particularly, in the a-axis, and β angle, in comparison to those of pristine CYCU-3 (a = 34.067 Å, b = 60.07 Å, c = 6.312 Å, α = 90.0°, β = 90.0°, and γ = 90.0°),[33] which may suggest that CYCU-3' 50_50 is a new structure of the original MOF. Unfortunately, CYCU-3' 50_50 structure is disordered along b-axis, as severe diffraction streaks along this direction were observed in the reconstructed 3D reciprocal lattice (Figure S4). Thus, this disorder together with the flexible behaviour of the crystals (bending, twisting and coiling) (Figure S4 a-c), avoid a direct structure solution using *c*RED data. For this reason, Pawley fit was applied to the PXRD data to confirm and refine the unit cell parameters (Figure S5). The refinement was conducted using a Pearson VII type peak profile function, followed by refinement of unit cells and zero-shift. R-value was converged to R_p = 0.110, R_{wp} = 0.0634, R_{exp} = 0.267, and GOF = 0.237. The high R_{exp} and low GOF values are due to the broad peaks caused by the disorder and preferred orientation. The new refined unit cell parameters (a = 16.971 Å, b = 64.039 Å, c = 6.694 Å, α = 90.0°, β = 94.447°, and γ = 90°) confirmed that CYCU-3' 50_50 changes to a new structure. Based on these data, an average structural model for CYCU-3' 50_50 was built (Figure S6). The crystal structure is based on AlO_6 corner-shared octahedra leading to 1D chains as in CYCU-3. However, there are more Al chains in the unit cell of CYCU-3' 50_50 than in CYCU-3 as the a-axis of the former is halved (a = 16.35 and 34.067 Å, respectively). As a consequence, CYCU-3' 50_50 framework is 61% more dense than that of pristine CYCU-3 (0.731 g/cm^{-3} and 0.453 g/cm^{-3}, respectively), resulting in a material with a lower BET surface

area (see the preparation of hybrid materials for more details). In addition, the new CYCU-3' 50_50 structure has 1D channels that represent the small pores of CYCU-3. On the other hand, the disordered nature of CYCU-3' 50_50 crystals (Figure S4) could be caused by the coordination of acetate instead of SDC ligands to the Al centres not only in the crystal surface but also in the inner structure creating defects (Figure 3a). This hypothesis is further supported by elemental analysis, where a high acetate/SDC ratio of 1.63 was found. To confirm the structural model, ED pattern simulation was applied (Figure 3b). The experimental ED pattern of CYCU-3' 50_50 (Figure 3b-I) was compared with CYCU-3' 50_50 average model (Figure 3b-III), and the simulated ED pattern of CYCU-3 (Figure 3b-II, generated from the previously reported CYCU-3 structure[33]). Extra diffraction rows are observed in Figures 3b-I, which agrees well with the pattern from CYCU-3' 50_50 average model (Figure 3b-II), while the simulated ED pattern of CYCU-3 lacks of these rows (Figure 3b-III). This suggests that the proposed model of CYCU-3' 50_50 is correct, and it is a different phase than original CYCU-3. However, the high degree of disorder found in CYCU-3' 50_50 may be caused by the previously mentioned ligand defects and/or by missing AlO_6 chains.

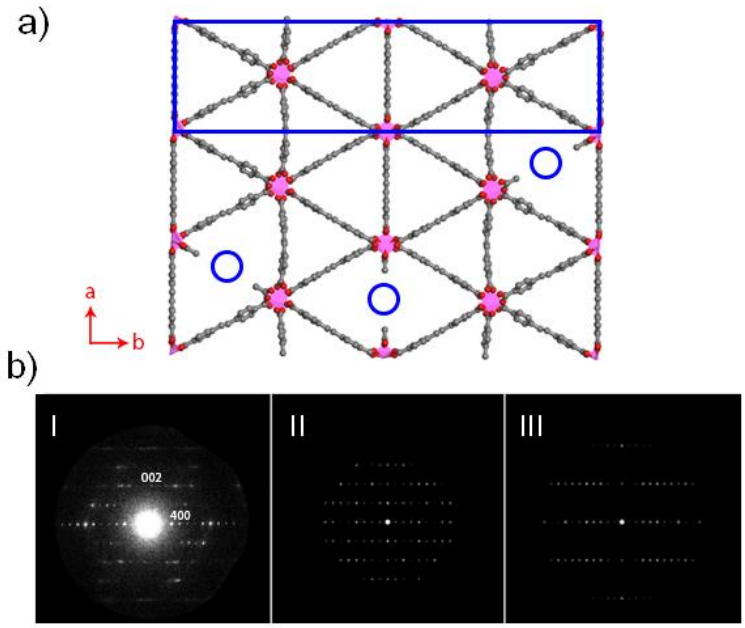

Figure 3. a) Proposed structural model of CYCU-3' 50_50 along c-axis. b) Experimental ED pattern of CYCU-3' 50_50 (I), and simulated ED pattern of CYCU-3' 50_50 (II) and CYCU-3 (III) (view along [001]).

Preparation of ALF794@CYCU-3 hybrid materials

In view of the previously discussed results, we used three CYCU-3 materials with different particle features for the loading of the photoactive CORM ALF794 [$Mo(CNCMe_2CO_2H)_3(CO)_3$] ($CNCMe_2CO_2H$ = 2-isocyano-2-methyl propionic acid). The potential influence that particle size and morphology exerted on the properties of the resulting ALF794@CYCU-3 CORMAs was analyzed. In particular, we selected: *i)* CYCU-3 20_0, comprising pseudospherical nanoparticles in the nanometric range (~ 100 nm); *ii)* CYCU-3 50_5, formed by bar-type particles with heterogeneous size and *iii)* CYCU-3' 50_50, which presents micrometric needles with a distorted and defective structure (Figure 4). These materials were scaled-up and an exhaustive washing

process was performed in order to remove the unreacted ligand molecules that may be trapped inside the cavities of the matrixes (see Experimental Section).

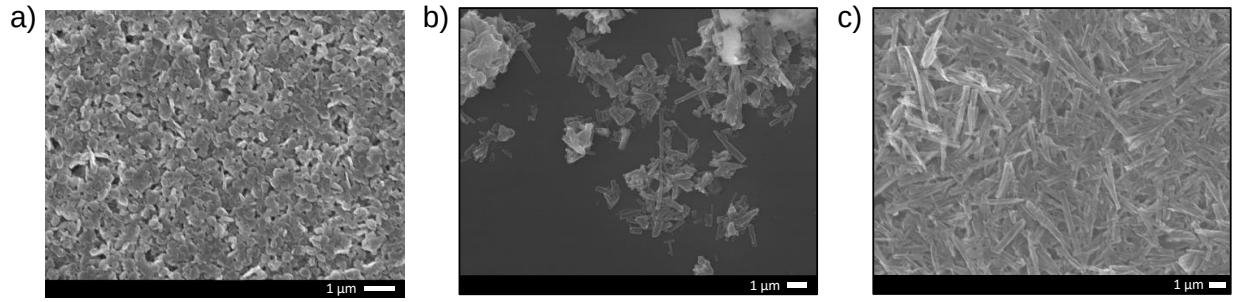

Figure 4. SEM images of selected CYCU-3 materials exhibiting: a) pseudospherical nanoparticles of CYCU-3 20_0, b) heterogeneous bar-like CYCU-3 50_5 particles and c) long CYCU-3' 50_50 needles.

Afterwards, the matrices were activated (150 °C under vacuum for 24 hours) and thermogravimetric analysis of the desolvated materials were recorded, confirming that, in all cases, CYCU-3 materials were free of ligand and/or solvent molecules as no mass loss was observed up to ~350 ºC (Figure S7). Regarding thermal stability, decomposition temperature increases with particle size (ca. 351, 408 and 473 ºC, for CYCU-3 20_0, CYCU-3 50_5 and CYCU-3' 50_50, respectively). In addition, we evaluated the permanent porosity of these materials by measuring the nitrogen adsorption isotherms at 77 K (Figure S8). In all cases, the isotherm profiles were characteristic of materials with both micro- and mesopores. Besides, CYCU-3 20_0 and CYCU-3 50_5 exhibited a similar BET surface (2225 and 2270 m^2 g^{-1}, respectively) than the previously reported for pristine CYCU-3[33] (2760 m^2 g^{-1}), while the adsorption capacity of CYCU-3' 50_50 was markedly lower (265 m^2 g^{-1}) probably due to its more dense framework compared to pristine CYCU-3 (see the structural studies for more

details). The pore size distribution of the different porous frameworks was also determined (Figure S9).

Once the selected CYCU-3 materials were characterized, we carried out the diffusion of the CO-prodrug by means of a solid-liquid impregnation strategy. All materials were suspended in a methanolic solution of ALF794 and the mixtures were stirred until complete evaporation of the solvent in order to force the incorporation of the drug into the pores (see Experimental Section). The resulting solids were thoroughly washed with MeOH and allowed to dry at room temperature. Infrared spectroscopy firstly confirmed the successful loading of ALF794 into the cavities of the three selected porous matrices (Figure 5, Figure S10). The characteristic stretching CO bands of ALF794 appeared slightly shifted in the hybrid materials compared to the pristine CORM. This small displacement is due to the confinement of the CORM molecules inside the pores as previously reported in literature.[36,37]

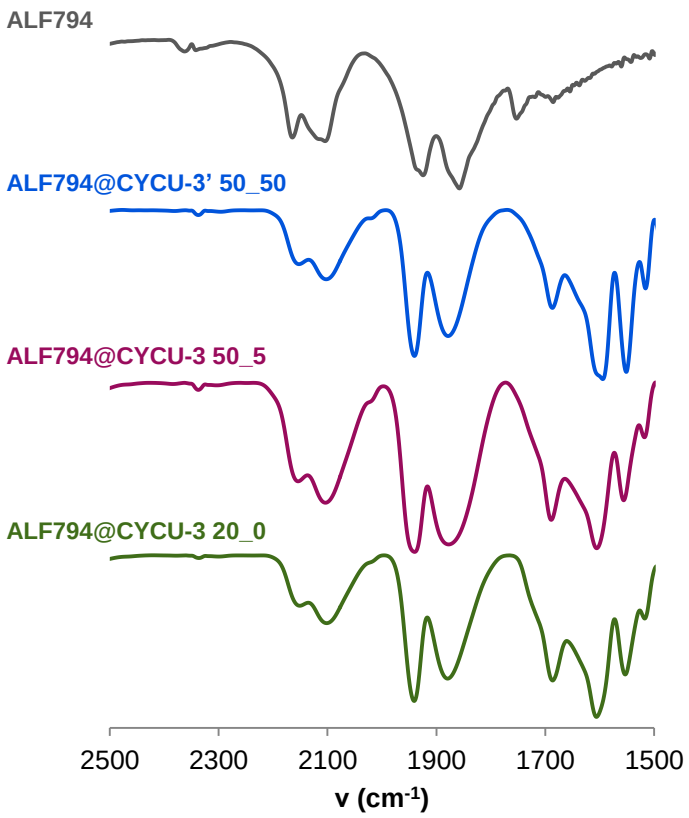

Figure 5. Selected region of FT-IR spectra of pristine ALF794 and hybrid materials ALF794CYCU-3 20_0, ALF794@CYCU-3 50_5 and ALF794@CYCU-3' 50_50, showing the characteristic CO stretching bands.

In addition, TEM images showed that no significant changes either in particle morphology or size took place after the adsorption process while EDX elemental mapping corroborated the homogeneous distribution of both molybdenum and aluminium elements over the particles (Figure 6).

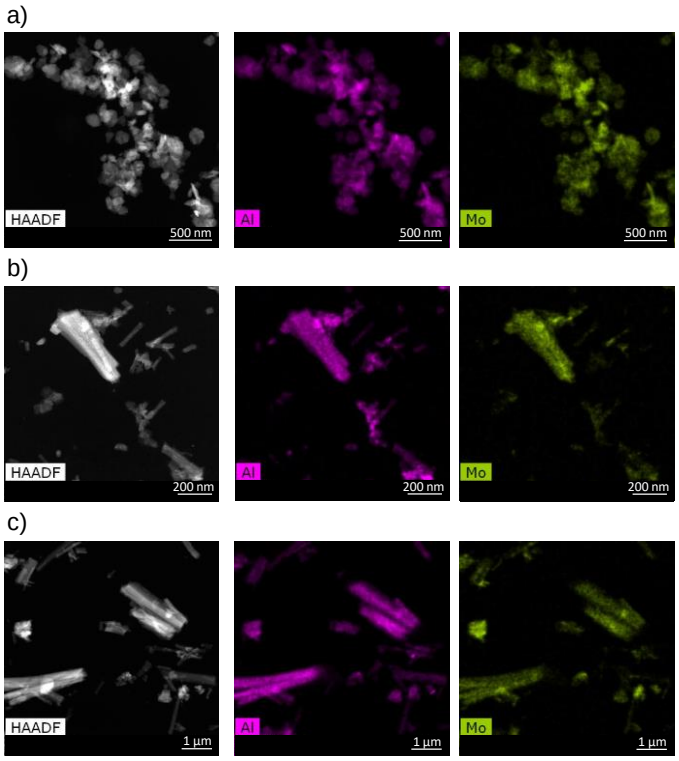

Figure 6. TEM images and EDX-elemental mapping confirming the incorporation of the CORM (Al: pink, Mo: green). a) ALF794@CYCU-3 20_0; b) ALF794@CYCU-3 50_5; c) ALF794@CYCU-3' 50_50.

The quantification of ALF794 loading was estimated by X-ray fluorescence analysis. In all cases, similar Mo/Al molar ratios were found (0.14, 0.20 and 0.19 for ALF794@CYCU-3 20_0, ALF794@CYCU-3 50_5 and ALF794@CYCU-3' 50_50, respectively), suggesting that particle size/morphology of the synthetized matrices do not have an appreciable influence on the total amount of loaded CO-prodrug. Moreover, the presence of defects in CYCU-3' 50_50 structure seems to favor the inclusion of the CORM in the pore structure, leading to a similar payload to that found for the other two prepared materials, which exhibit significant higher BET surface areas (see above).

The hybrid materials were also characterized by PXRD (Figure S11). Thus, ALF794@CYCU-3 50_5 and ALF794@CYCU-3' 50_50 solids showed similar diffraction patterns to those of the corresponding empty matrixes, confirming their stability under the drug-loading conditions. On the contrary, ALF794@CYCU-3 20_0 nanoparticles exhibited a slight degradation as two new reflections appeared in the PXRD pattern attributed to free H_2SDC ligand. These results point towards direct relationship between particle size and chemical stability of the hybrid materials. For this reason, ALF794@CYCU-3 20_0 was not considered for further studies.

Evaluation of ALF794@CYCU-3 hybrid materials as potential CORMAs

In order to test the potential biological application as CORMAs of ALF794@CYCU-3 50_5 and ALF794@CYCU-3' 50_50, their photoinduced CO release properties were firstly investigated in solution (10 mM PBS, 37 °C) by UV-vis spectroscopy using the myoglobin assay.[11] Although both hybrid materials released appreciable amounts of CO (0.46 and 0.24 mmol of CO per mmol of CORM upon 24 hours of irradiation with visible light, Figure S12, molybdenum leaching was also detected (94% and 25%, respectively, after 6 hours of incubation with no further leaching in the next 72 hours) (Table S1). The high extent of metal leaching from ALF794@CYCU-3 50_5 might be attributed to its smaller particle size, which unfortunately leads to a high degradation of the framework in phosphate saline buffer. In contrast, ALF794@CYCU-3' 50_50 shows a significantly lower metal leaching (25% of Mo) related to its less porous structure and larger particle size. [27,28,30] Taking into account the later fact, ALF794@CYCU-3' 50_50 is the only hybrid material that can be considered as a real CORMA in solution.

In order to further explore the ability of these hybrid systems as CORMAs, we decided to study their CO-delivery properties in the solid state, envisaging their potential use for topical applications (i.e. anti-inflammatory bandages). In this context, it should be highlighted the

previously reported innovative application of photoactive CORMs for topical treatment of epidermal cancer. Indeed, CORM-2, $[Ru_2Cl_4(CO)_6]$, lotions were shown to reduce the acute and chronic inflammation and tumor multiplicity in hairless mice with induced photocarcinogenesis.[38] Thus, an in-line CO detector was customized to measure the CO released from ALF794@CYCU-3 50_5 and ALF794@CYCU-3' 50_50 solid matrixes (Figure S13). In particular, both hybrid materials were spin-coated and irradiated at 250-385 nm with 50 mW cm^{-2} of light power to promote the CO release. The delivered CO was transferred using N_2 as carrier gas to the in-line detector. The CO release efficiencies of the ALF794-loaded materials were compared to that of free CORM (Figure 7). Thus, pristine ALF794 behaves also as a photoCORM in the solid state, releasing 0.42 mmol of CO per mmol of CORM after 220 min (photoreleasing efficiency: 42%). In addition, both hybrid materials retain the photoactivable properties of the molybdenum tricarbonyl complex showing an average CO delivery of 0.44 and 0.35 mmol of CO per mmol of CORM (44 and 35% of CO release efficiency) for ALF794@CYCU-3 50_5 and ALF794@CYCU-3' 50_50, respectively.

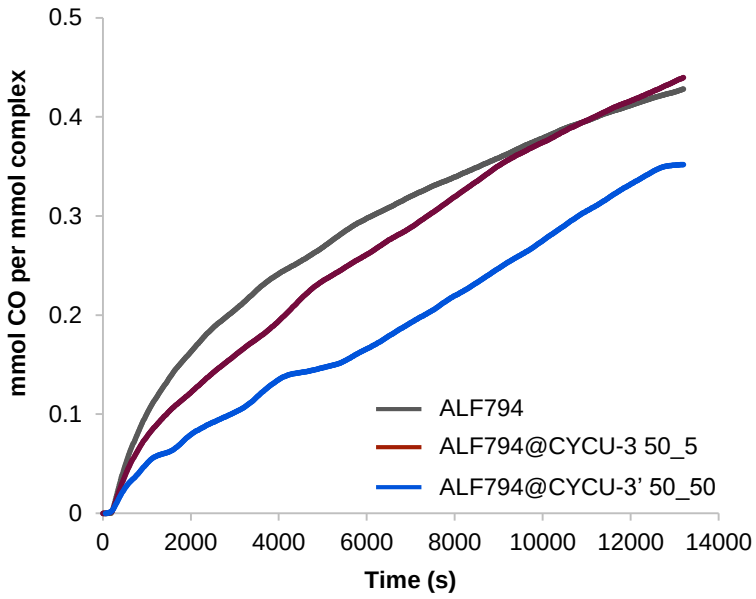

Figure 7. CO delivery kinetic profiles of free ALF794 (grey curve), ALF794@CYCU-3 50_5 (purple curve) and ALF794@CYCU-3' 50_50 (blue curve) upon photoactivation in the solid state.

The corresponding CO delivery efficiencies were calculated based on the higher lability of one of the three CO ligands per $[Mo(CO)_3(CNCMe_2CO_2H)_3]$ complex, as previously reported for this CORM.[30] The slightly lower efficiency found in ALF794@CYCU-3' 50_50 may be explained taking into account that light penetration is limited by the thickness of the crystals. Consequently, ALF794@CYCU-3' 50_50 micrometric crystals may partially hinder the photoactivation of ALF794 CO-releasing molecule in comparison to those of ALF794@CYCU-3 50_5, which exhibits a significantly smaller particle size.

CONCLUSIONS

In this work, we have used the coordination modulation method to successfully prepare several CYCU-3 materials with different particle size and morphology, ranging from pseudo-spherical nanoparticles of ~100 nm to elongated particles of several microns. Surprisingly, when we used a modulator concentration fifty timer greater than that of the ligand, a new crystalline phase (CYCU-3' 50_50) was obtained. In particular, unit cell parameters and space group of CYCU-3' 50_50 were determined from cRED data and the former were further refined against PXRD data using Pawley method, suggesting that CYCU-3' 50_50 is probably an analogous structure of pristine CYCU-3. Unfortunately, the poor crystallinity of the material prevented a direct structure solution. For this reason, a possible structural model for CYCU-3' 50_50 was built and the corresponding simulated ED patterns fitted well with the experimental ones. In addition, we have loaded the bioactive CO-prodrug ALF794 in three selected CYCU-3 materials (CYCU-3 20_0, CYCU-3 50_5 and CYCU-3' 50_50) and investigated the influence of MOF's features over the properties of the resulting CORMAs. We observed that the nanometric nature of CYCU-3 20_0 was responsible for the partial degradation of the matrix under the drug-loading conditions. For this reason, this material was not considered for further studies. Regarding ALF794@CYCU-3 50_5 and ALF794@CYCU-3' 50_50 hybrid materials showing particles in the micrometric range, CO delivery was evaluated in solution and in solid state envisaging their potential use for topical therapeutic applications. Our results demonstrated that both hybrid materials retained the photoactive properties of pristine CORM with ALF794@CYCU-3' 50_50 exhibiting the highest retention of metal fragments in PBS reported to date for a MOF-based CO releasing material, which makes it a real CORMA.

ASSOCIATED CONTENT

Supporting Information. SEM and TEM images, X-ray powder diffractograms, additional structural data, TG analysis, Infrared spectra, N_2 adsorption isotherms and pore size distribution, CO-delivery assays in solution, Mo-leaching studies.

AUTHOR INFORMATION

Corresponding Author

*Elisa Barea, e-mail: ebaream@ugr.es

ORCID:

Francisco J. Carmona: 0000-0001-8489-6446

Carlos C. Romão: 0000-0001-5061-3743

Zhehao Huang: 0000-0002-4575-7870

Carmen R. Maldonado: 0000-0002-4958-6052

Shuhei Furukawa: 0000-0003-3849-8038

Elisa Barea: 0000-0001-9895-1047

Author Contributions

The manuscript was written through contributions of all authors. All authors have given approval to the final version of the manuscript.

ACKNOWLEDGMENT

The Spanish Ministry of Economy and Competitivity and UE Feder Program (project CTQ2014-53486R and CTQ2017-84692-R), Japan Society for the Promotion of Science (EB, Invitation Fellowship (Long-Term) L-14529), University of Granada (CRM, Reincorporación Plan Propio),

and COST action CM1105 are gratefully acknowledged for generous funding. This study was partially supported by the “Unidad de Excelencia de Química aplicada a biomedicina y medioambiente” (University of Granada). The authors thank Proterris (Portugal) Lda for providing ALF794 and H. Jeremias for preparing it. The NMR data was acquired at CERMAX, ITQB-NOVA, Oeiras, Portugal. The authors thank iCeMS Analysis Centers for access to the experimental facilities. Structural analyses were supported by the 3DEMNATUR project from the Knut and Alice Wallenberg Foundation (KAW) and the MATsynCELL project through Röntgen-Ångström Cluster, the Swedish Research Council (VR).

REFERENCES

(1) Moncada, S. Nitric Oxide: Discovery and Impact on Clinical Medicine. *J. R. Soc. Med.* **1999**, *92*, 164–169.

(2) Ignarro, L. J.; Cirino, G.; Casini, A.; Napoli, C. Nitric Oxide as a Signaling Molecule in the Vascular System: An Overview. *J. Cardiovasc. Pharmacol.* **1999**, *34*, 879–886.

(3) Motterlini, R.; Otterbein, L. E. The Therapeutic Potential of Carbon Monoxide. *Nat. Rev. Drug Discov.* **2010**, *9*, 728–743.

(4) Li, L.; Rose, P.; Moore, P. K. Hydrogen Sulfide and Cell Signaling. *Annu. Rev. Pharmacol. Toxicol.* **2011**, *51*, 169–187.

(5) Fukuto, J. M.; Carrington, S. J.; Tantillo, D. J.; Harrison, J. G.; Ignarro, L. J.; Freeman, B. A.; Chen, A.; Wink, D. A. Small Molecule Signaling Agents: The Integrated Chemistry and Biochemistry of Nitrogen Oxides, Oxides of Carbon, Dioxygen, Hydrogen Sulfide, and Their Derived Species. *Chem. Res. Toxicol.* **2012**, *25*, 769–793.

(6) Motterlini, R.; Foresti, R. Biological Signaling by Carbon Monoxide and Carbon Monoxide-Releasing Molecules. *Am. J. Physiol. Cell Physiol.* **2017**, *312*, C302–C313.

(7) Heinemann, S. H.; Hoshi, T.; Westerhausen, M.; Schiller, A. Carbon Monoxide-Physiology, Detection and Controlled Release. *Chem. Commun.* **2014**, *50*, 3644–3660.

(8) ClinicalTrials.gov. Role of CarbonMonoxyde in the Ex Vivo Lung Perfusion Reconditionning, NCT02032082 First Received: January 2014; Last Verified: January 2017. Study Active.

(9) ClinicalTrials.gov. CO as a Stimulant for Mitochondrial Biogenesis in Human Cardiac Muscle, NCT01727167 First Received: November, 2012; Last Verified: January 2017. Study Completed.

(10) Schatzschneider, U. Novel Lead Structures and Activation Mechanisms for CO-Releasing Molecules (CORMs). *Br. J. Pharmacol.* **2015**, *172*, 1638–1650.

(11) Motterlini, R.; Clark, J. E.; Foresti, R.; Sarathchandra, P.; Mann, B. E.; Green, C. J. Carbon Monoxide-Releasing Molecules: Characterization of Biochemical and Vascular Activities. *Circ. Res.* **2002**, *90*, e17–e24.

(12) Romão, C. C.; Blättler, W. A.; Seixas, J. D.; Bernardes, G. J. L. Developing Drug Molecules for Therapy with Carbon Monoxide. *Chem. Soc. Rev.* **2012**, *41*, 3571–3583.

(13) García-Gallego, S.; Bernardes, G. J. L. Carbon-Monoxide-Releasing Molecules for the Delivery of Therapeutic CO in Vivo. *Angew. Chem. Int. Ed.*. 2014, *53,* 9712–9721.

(14) Inaba, H.; Fujita, K.; Ueno, T. Design of Biomaterials for Intracellular Delivery of Carbon Monoxide. *Biomater. Sci.* **2015**, *3*, 1423–1438.

(15) Kautz, A. C.; Kunz, P. C.; Janiak, C. CO-Releasing Molecule (CORM) Conjugate Systems. *Dalt. Trans.* **2016**, *45*, 18045–18063.

(16) Nguyen, D.; Boyer, C. Macromolecular and Inorganic Nanomaterials Scaffolds for Carbon Monoxide Delivery: Recent Developments and Future Trends. *ACS Biomater. Sci. Eng.* **2015**, *1*, 895–913.

(17) Hasegawa, U.; Van Der Vlies, A. J.; Simeoni, E.; Wandrey, C.; Hubbell, J. A. Carbon

Monoxide-Releasing Micelles for Immunotherapy. *J. Am. Chem. Soc.* **2010**, *132*, 18273–18280.

(18) Chakraborty, I.; Carrington, S. J.; Hauser, J.; Oliver, S. R. J.; Mascharak, P. K. Rapid Eradication of Human Breast Cancer Cells through Trackable Light-Triggered CO Delivery by Mesoporous Silica Nanoparticles Packed with a Designed photoCORM. *Chem. Mater.* **2015**, *27*, 8387–8397.

(19) Dördelmann, G.; Pfeiffer, H.; Birkner, A.; Schatzschneider, U. Silicium Dioxide Nanoparticles as Carriers for Photoactivatable Co-Releasing Molecules (PhotoCORMs). *Inorg. Chem.* **2011**, *50*, 4362–4367.

(20) Tabe, H.; Fujita, K.; Abe, S.; Tsujimoto, M.; Kuchimaru, T.; Kizaka-Kondoh, S.; Takano, M.; Kitagawa, S.; Ueno, T. Preparation of a Cross-Linked Porous Protein Crystal Containing Ru Carbonyl Complexes as a CO-Releasing Extracellular Scaffold. *Inorg. Chem.* **2015**, *54*, 215–220.

(21) Reddy G., U.; Liu, J.; Hoffmann, P.; Steinmetzer, J.; Görls, H.; Kupfer, S.; Askes, S. H. C.; Neugebauer, U.; Gräfe, S.; Schiller, A. Light-Responsive Paper Strips as CO-Releasing Material with a Colourimetric Response. *Chem. Sci.* **2017**, *8*, 6555–6560.

(22) Pinto, M. N.; Chakraborty, I.; Sandoval, C.; Mascharak, P. K. Eradication of HT-29 Colorectal Adenocarcinoma Cells by Controlled Photorelease of CO from a CO-Releasing Polymer (photoCORP-1) Triggered by Visible Light through an Optical Fiber-Based Device. *J. Control. Release* **2017**, *264*, 192–202.

(23) Chakraborty, I.; Jimenez, J.; Mascharak, P. K. CO-Induced Apoptotic Death of Colorectal

Cancer Cells by a Luminescent photoCORM Grafted on Biocompatible Carboxymethyl Chitosan. *Chem. Commun.* **2017**, *53*, 5519–5522.

(24) Horcajada, P.; Gref, R.; Baati, T.; Allan, P. K.; Maurin, G.; Couvreur, P.; Férey, G.; Morris, R. E.; Serre, C. Metal-Organic Frameworks in Biomedicine. *Chem. Rev.* **2012**, *112*, 1232–1268.

(25) Tsuruoka, T.; Furukawa, S.; Takashima, Y.; Yoshida, K.; Isoda, S.; Kitagawa, S. Nanoporous Nanorods Fabricated by Coordination Modulation and Oriented Attachment Growth. *Angew. Chem. Int. Ed.* **2009**, *48*, 4739–4743.

(26) Ma, M.; Noei, H.; Mienert, B.; Niesel, J.; Bill, E.; Muhler, M.; Fischer, R. A.; Wang, Y.; Schatzschneider, U.; Metzler-Nolte, N. Iron Metal-Organic Frameworks MIL-88B and NH2-MIL-88B for the Loading and Delivery of the Gasotransmitter Carbon Monoxide. *Chem. Eur. J.* **2013**, *19*, 6785–6790.

(27) Carmona, F. J.; Rojas, S.; Sánchez, P.; Jeremias, H.; Marques, A. R.; Romão, C. C.; Choquesillo-Lazarte, D.; Navarro, J. A. R.; Maldonado, C. R.; Barea, E. Cation Exchange Strategy for the Encapsulation of a Photoactive CO-Releasing Organometallic Molecule into Anionic Porous Frameworks. *Inorg. Chem.* **2016**, *55*, 6525–6531.

(28) Diring, S.; Carné-Sánchez, A.; Zhang, J.; Ikemura, S.; Kim, C.; Inaba, H.; Kitagawa, S.; Furukawa, S. Light Responsive Metal-Organic Frameworks as a Controllable CO-Releasing Cell Culture Substrate. *Chem. Sci.* **2017**, *8*, 2381–2386.

(29) Marques, A. R.; Kromer, L.; Gallo, D. J.; Penacho, N.; Rodrigues, S. S.; Seixas, J. D.; Bernardes, G. J. L.; Reis, P. M.; Otterbein, S. L.; Ruggieri, R. A.; Gonçalves, A. S. G.;

De Matos, M. N.; Bento, I; Otterbein, L. E.; Blättler, W. A.; Romão, C. C. Generation of Carbon Monoxide Releasing Molecules (CO-RMs) as Drug Candidates for the Treatment of Acute Liver Injury: Targeting of CO-RMs to the Liver. *Organometallics* **2012**, *31*, 5810–5822.

(30) Carmona, F. J.; Rojas, S.; Romao, C.; Navarro, J. A. R.; Barea, E.; Maldonado, C. R. One-Pot Preparation of a Novel CO-Releasing Material Based on a CO-Releasing Molecule@Metal-Organic Framework System. *Chem. Commun.* **2017**, *53*, 6581–6584.

(31) Giménez-Marqués, M.; Hidalgo, T.; Serre, C.; Horcajada, P. Nanostructured Metal-Organic Frameworks and Their Bio-Related Applications. *Coord. Chem. Rev.* **2016**, *307*, 342–360.

(32) Liu, B.; Vellingiri, K.; Jo, S.-H.; Kumar, P.; Ok, Y. S.; Kim, K.-H. Recent Advances in Controlled Modification of the Size and Morphology of Metal-Organic Frameworks. *Nano Res.* **2018**, *11*, 4441–4467.

(33) Lo, S.-H.; Chien, C.-H.; Lai, Y.-L.; Yang, C.-C.; Lee, J. J.; Raja, D. S.; Lin, C.-H. A Mesoporous Aluminium Metal–organic Framework with 3 Nm Open Pores. *J. Mater. Chem. A* **2013**, *1*, 324–329.

(34) Simon-Yarza, T.; Rojas, S.; Horcajada, P.; Serre, C. 4.38 The Situation of Metal-Organic Frameworks in Biomedicine; Ducheyne, P. B. T.-C. B. I. I., Ed.; Elsevier: Oxford, 2017; pp 719–749.

(35) Orellana-Tavra, C.; Marshall, R. J.; Baxter, E. F.; Lázaro, I. A.; Tao, A.; Cheetham, A. K.; Forgan, R. S.; Fairen-Jimenez, D. Drug Delivery and Controlled Release from

Biocompatible Metal–organic Frameworks Using Mechanical Amorphization. *J. Mater. Chem. B* **2016**, *4*, 7697–7707.

(36) Gonzales, M. A.; Han, H.; Moyes, A.; Radinos, A.; Hobbs, A. J.; Coombs, N.; Oliver, S. R. J.; Mascharak, P. K. Light-Triggered Carbon Monoxide Delivery with Al-MCM-41-Based Nanoparticles Bearing a Designed Manganese Carbonyl Complex. *J. Mater. Chem. B* **2014**, *2*, 2107–2113.

(37) Carmona, F. J.; Jiménez-Amezcua, I.; Rojas, S.; Romão, C. C.; Navarro, J. A. R.; Maldonado, C. R.; Barea, E. Aluminum Doped MCM-41 Nanoparticles as Platforms for the Dual Encapsulation of a CO-Releasing Molecule and Cisplatin. *Inorg. Chem.* **2017**, *56*, 10474–10480.

(38) Allanson, M.; Reeve, V. E. Carbon Monoxide Signalling Reduces Photocarcinogenesis in the Hairless Mouse. *Cancer Immunol. Immunother.* **2007**, *56*, 1807–1815.

TOC